

Supplemental Material

**Time-dependent inversion of three-component continuous GPS for
steady and transient sources in northern Cascadia
Geophysical Research Letters, doi:10.1029/2008GL036784, 2009.**

Robert McCaffrey

Dept. of Earth and Environmental Science, Rensselaer Polytechnic Institute
Troy NY 12180 mccafri@rpi.edu

Geodetic time series contain several signals (Fig. A1). The goal of the method outlined here is to separate the components that are due to steady tectonic motions (rotations, locking strains and anelastic strains) from the transient motions due to ephemeral sources such as slow slip events, earthquakes, afterslip and volcanic events. The approach differs from earlier methods in that the parameters describing the steady motions are estimated simultaneously with the transients.

The geodetic signals due to these sources are strongly correlated in time and space. The spatial correlation is exploited in order to estimate the steady motions of sites that have short or sporadic occupation histories (such as survey-mode sites or relatively new continuous sites). This spatial correlation for the steady-state part of the signal is realized through a block model in which elastic-plastic portions of the crust (blocks) move relative to each other causing elastic strain at their boundary faults. The blocks can also deform internally through a uniform horizontal strain rate tensor. For simplicity I call this type of model ‘RLPS’ indicating Rotation, Locking and Permanent Stain. Much of the block modeling technique used here is described in the DEFNODE manual at www.rpi.edu/~mccafri/defnode. DEFNODE is designed to use GPS velocity and displacement vectors. It has been modified to use the time series directly in addition to the velocities derived from them. Here, this material is reviewed and the new methods relating to time series analysis are described.

The RLPS model forms the long-term constant (or ‘steady-state’ over the time period being examined) geodetic surface velocities via a combination of crustal block rotations, elastic strain rates from locked faults and distributed permanent strain rates. The steady part of the problem is represented by a linear time series of discrete observations of position X :

$$X_{ij}(t) = X_{ij}^0 + V_{ij} (t - t_o) + \varepsilon_{ij}(t) \quad (1)$$

where X_{ij}^0 is the initial position of component i (east, north and up) of site j at time $t = t_o$, V_{ij} is the i^{th} component of secular velocity of site j and $\varepsilon_{ij}(t)$ represents other signals. Commonly, the velocity V is estimated by finding the best-fit slope for each time series individually. Here V is derived from the RLPS model which takes advantage of the strong spatial correlation of velocities among nearby geodetic sites due to the inherent long-wavelengths of Earth deformation. In a sense, spatial smoothing of the secular velocities is applied via a physical model rather than by regularization parameters used in other methods. The initial positions X_{ij}^0 are estimated as part of the inversion.

Inter-event locking distribution. The locking on the Cascadia thrust in the time between slow slip events is parameterized by a function in the downdip direction w as described in McCaffrey et al.

(2007) and in the DEFNODE users' manual. Nodes were defined as the intersections of the plate interface (McCrory et al., 2002) at specified depths with 29 vertical planes going through points at the deformation front and approximately perpendicular to the deformation front (Fig. A2). Along each downdip profile a locking parameter ϕ was assumed to vary with depth as described by McCaffrey et al. (2007). This function follows Wang *et al.* (2003) in that $\phi = 1.0$ (full locking) at depths shallower than the top, z_u , of what they call the 'effective transition zone' (ETZ) and $\phi = 0.0$ (free slip) at depths below the bottom, z_l , of the ETZ. Within the ETZ

$$\phi(z) = [\exp(-z'/\gamma) - \exp(-1/\gamma)] / [1 - \exp(-1/\gamma)] \quad (2)$$

where $z' = (z - z_u) / (z_l - z_u)$ and γ is a shape factor. I modified Wang's representation of the depth distribution of locking to allow for a more general case. Equation 2, in addition to constraining ϕ to decrease with depth, forces the slope $d\phi/dz$ to increase or remain approximately constant with depth (see Wang *et al.*, their Fig 8). To allow the slope to decrease with depth, I use a new parameter, γ' , and make the substitution in (2) of $\gamma = \gamma'$ when $\gamma' \leq 5$, and $\gamma = \gamma' - 10$ when $5 < \gamma' \leq 10$. For values of γ' between 0 and 5, $\phi(z)$ is given by (2) and for γ' between 5 and 10, $\phi(z)$ is reflected about the ϕ and z axes (McCaffrey et al., 2007; Fig. 7a). The inter-event locking that is applied in the backslip method is $-\phi V$ where V is the relative velocity across the fault determined by the block angular velocities. I use the backslip method and an elastic half-space. Unlike McCaffrey et al. (2007), locking on crustal faults was not estimated here.

Block model. The block model used is similar to that of McCaffrey et al. (2007) but is limited to the region around western Washington and southwest British Columbia. The model comprises 7 blocks (Fig. 2); Juan de Fuca plate (JdFa), northern Oregon Coast Ranges (NoCR), Olympics (Olym), southern Vancouver Island (SoVI), Wenatchee (Wena), Puget Sound (Pugt), Canadian Inter-montane belt (CIMB) and Eastern Oregon (EOre) with North America as the reference frame. Motion of JdFa relative to North America was fixed (244.6°E , 33.8°N , $-1.52^\circ/\text{Myr}$; McCaffrey et al., 2007). CIMB was fixed to North America, and the angular velocities of the remaining blocks were adjusted to fit the time series. Uniform horizontal strain rate tensors were also estimated for the SoVI, Olym and Pugt blocks. Unlike McCaffrey et al. (2007), I did not use geologic fault slip rates or slip vectors in this inversion.

Transient Slip Distribution. The distribution of transient slip on the fault can be represented in a variety of ways in the methodology. The main type of transient to be addressed in this application is slow slip but the method at present can also be applied to earthquakes, with or without afterslip, and time-dependent volcanic sources such as a Mogi source. Slow-slip events (SSE) are thought to be due to slip on fault planes, much like earthquakes, but occur slowly enough to not radiate detectable seismic waves, except perhaps as non-volcanic tremor. The surface displacements from slow slip are very similar to what earthquakes produce so are thought to be slip on fault planes.

Inversions generally solve for slip on discrete patches of the fault and use smoothing (regularization) to specify the covariance between adjacent and nearby patches that are usually not independently resolved (e.g., Segall and Matthews, 1997; Fukuda et al., 2008; Szeliga et al. 2008). Here, as an alternative, I use simple functions to describe the spatial and temporal distributions of slip on the fault surface (Figs. A3 and A4). The program does allow for distributed slip at each node on the fault (Fig.

A3d) which requires some smoothing as in the other methods. The slip rate, s , on the fault during an event is described by:

$$s(x, w, t) = A \ X(x) W(w) S(t) \quad (3)$$

where x is along-strike position on the fault, w is the down-dip position, t is time, and A is the amplitude.

Here I represent slip during the transient event in ways that allow it to be described with a small number of free parameters. It can be described by a simple 2-dimensional Gaussian function of position (Fig. A3a):

$$X(x') = \exp(-\frac{1}{2} [(x' - X_c)/X_s]^2) \quad (4a)$$

$$W(w') = \exp(-\frac{1}{2} [(w' - W_c)/W_s]^2) \quad (4b)$$

where X_c is the along-strike center of the slip function and X_s represents its along-strike spread, and W_c and W_s are the down-dip center and spread. The coordinates (x', w') are rotated about an angle θ relative to (x, w) to allow the Gaussian slip distribution to be rotated relative to the x -axis. In this case the spatial distribution of slip is given by the free parameters X_c , X_s , W_c , W_s , and θ (X_c and W_c are in km but are converted to geographic position in degrees of longitude and latitude, X_s and W_s are in km, θ is in degrees relative to positive x -axis).

Another representation is by a series of one-dimensional (in depth) Gaussian distributions (Fig. A3b) along down-dip profiles (the down-dip profiles are as described above for the inter-seismic locking representation). In this case the slip rate on the fault is:

$$S(z) = A \ exp(-\frac{1}{2} [(z - z_o)/z_s]^2) \quad (5)$$

where z is depth, z_o is the mean depth and z_s is the spread. Each profile has as free parameters A , z_o and z_s and along-strike smoothing can be applied.

An alternative parameterization of the spatial slip is by using a polygon within which slip is nominally uniform (Fig. A3c) and solving for the vertices of the polygon and the slip amplitude. The vertices of the polygon are found by the distance of each from a central point in a given azimuth on the fault plane. The central point is within the slip zone and the azimuths are evenly spaced. For this application, the central point is fixed (based on earlier inversions of more general slip distributions) and the free parameters are the radial distances of each vertex from it. For these events I use 10 vertices of the polygon so the 10 radii lengths are the free parameters. The amplitude is also a free parameter. A small (10%) gradient in slip is applied from the central point to the edge to avoid zero derivatives for the lengths of the radial arms. (If the slip rate were truly constant within the polygon, the change in surface displacement with respect to a change in the length of an arm could be zero because the fault is discretized at nodes.)

Finally, the slip distribution can be represented by a grid of node points (Fig. A3d). The amplitude of slip is estimated at each node and can be smoothed in the along strike and down-dip directions.

The time dependence $S(t)$ of the slow slip event can be set to an impulse, a Gaussian function, a boxcar function or a series of overlapping triangles (Fig. A4). The impulse time history is used for earthquakes and amplitude is the one free parameter. The Gaussian time function (Fig. A4b) has the form

$$S(t) = A \exp(-\frac{1}{2} [(t-T_o)/T_s]^2) \quad (6)$$

where A is the amplitude in mm/yr, T_o is the origin time in years and T_s is the time spread in years. The boxcar function (Fig. A4c) has free parameters of amplitude, starting time and duration. It results in a linear displacement history.

The time history of overlapping triangles (Fig A4d) is as done for earthquake time functions (e.g., Nabelek, 1984) -- for a slow slip event the free parameters are T_o , the origin time, and the triangle amplitudes A_i , ($i = 1, N$ where N is the number of triangles in the time function; A is given in mm/yr). For all events in this paper, triangular time histories are used and the rise-time of the triangle (τ) is fixed at 7 days. A test inversion in which $\tau = 4$ days is discussed below.

The slip history on the fault is found by integrating $S(t)$ over time (Fig. A4) and the surface displacement history is then calculated by applying the appropriate Green's functions.

Inversion. Inversions were done with a combination of grid search and simulated annealing (Press et al., 1989). The problem is non-linear because the fault locking depends on the product of two free parameters, or is derived from them. These are the slip fraction ϕ , derived from the locking parameters, and the slip velocity V , which is derived from the angular velocity parameters. The quantity that is minimized is the sum of the reduced chi-square of the weighted misfit residuals plus any penalties that are assessed for exceeding parameter bounds. For example, the slip fraction should fall in the range $0 \leq \phi \leq 1$ during the inter-event time so that fault locking is neither opposite nor faster than relative block motion.

Parameter uncertainties are estimated by a linearization at the best-fit parameter values. The derivatives dO_i/dP_j ($i = \text{observation O index}$, $j = \text{parameter P index}$) are calculated by finite differences. The *a posteriori* parameter covariance matrix is $(D^T C^{-1} D)^{-1}$ where D is the matrix of derivatives ($T = \text{transpose}$) and C is the data covariance matrix whose diagonal is the variance of the observations. For the inversions here the reduce chi-square of the misfit residuals were approximately unity, suggesting that the observation uncertainties are scaled correctly. However, the formal parameter uncertainties are likely underestimated due to the linearization.

For the RLPS model there are 3 free parameters for the angular velocity of a block, 3 free parameters describing a uniform horizontal strain rate tensor, and fault locking parameters. Here, where locking was modeled only on the Cascadia thrust, there were 16 independent profiles each with 3 independent parameters; z_u , z_l , and γ' (though there are 29 profiles, some adjacent ones were forced to have the same parameters). The Cascadia RLPS model had 6 angular velocities and 3 strain tensors for a total of 75 free parameters. For the GPS time series, one free parameter for each site-component is used to

estimate the offset X_o . I use 3-components for 53 sites giving 159 offset parameters. The inversion (P137) in which no transients were used had 234 free parameters. In total there were 247,134 observations used (each observation is the ENU component of position of a site on a day). The reduced chi-square χ^2 for this model was 1.146.

Poles for uncorrected model (no slow slip)

Block	Longitude	Latitude	Omega	SigOm	Emax	Emin	Az.
Eore	246.94	45.35	-0.407	0.006	0.1	0.0	100.6
NoCR	272.32	36.39	-0.150	0.016	4.4	0.1	120.7
Olym	243.34	47.01	-0.625	0.021	0.2	0.1	117.4
Pugt	292.38	9.56	-0.047	0.006	17.8	0.2	140.6
SoVI	276.77	7.31	-0.055	0.005	9.6	0.4	146.8
Wena	142.92	6.26	0.033	0.000	58.9	0.2	42.7

Omega is the rotation rate in $^\circ/\text{Myr}$. Emax and Emin are the error ellipse semi-major and semi-minor axes in degrees and Az is the azimuth of Emax.

Strain rates for uncorrected model (no slow slip)

Block	Long.	Lat.	E1	SigE1	E2	SigE2	A1	SigA1
Olym	236.5	47.5	-17.9	0.4	15.4	1.0	0.6	0.7
Pugt	238.0	47.8	-3.5	0.3	-1.6	0.3	-41.4	7.2
SoVI	236.0	49.0	-9.1	0.3	-3.4	0.3	-101.3	1.6

Strain rates are in $10^{-9}/\text{yr}$. E1 is the most compressive; E2 is least compressive; A1 is the azimuth of E1.

The second model (P078) shown in the text includes four slow slip events. Each slow slip event was represented by an origin time, 2 triangular time function elements (the 2008 event had 3), 10 radial distances for the slip distribution, one slip amplitude, a migration rate and a migration azimuth. In addition to the 234 parameters from the RLPS model, these additional 65 parameters resulted in a total of 295. The resulting $\chi^2 = 1.106$ which is $\sim 3.5\%$ lower than the model without transients.

Poles for SSE- corrected model

Block	Longitude	Latitude	Omega	SigOm	Emax	Emin	Az.
Eore	246.88	45.23	-0.406	0.006	0.1	0.0	101.5
NoCR	270.94	37.42	-0.159	0.013	3.3	0.1	119.3
Olym	242.61	47.16	-0.711	0.022	0.2	0.1	115.0
Pugt	284.54	10.81	-0.053	0.009	19.1	0.2	142.6
SoVI	260.49	28.05	-0.098	0.008	3.3	0.1	145.5
Wena	311.40	3.25	-0.034	0.008	57.0	0.2	137.9

Omega is the rotation rate in $^\circ/\text{Myr}$. Emax and Emin are the error ellipse semi-major and semi-minor axes in degrees and Az is the azimuth of Emax.

Strain rates for SSE-corrected model

Block	Long.	Lat.	E1	SigE1	E2	SigE2	A1	SigA1
Olym	236.5	47.5	-18.9	0.4	18.4	1.0	0.2	0.6
Pugt	238.0	47.8	-4.9	0.3	-4.1	0.4	-48.9	19.8
SoVI	236.0	49.0	-4.7	0.2	-4.1	0.2	-33.0	16.8

Strain rates are in 10^{-9} /yr. E1 is the most compressive; E2 is least compressive; A1 is the azimuth of E1.

Slow slip event parameters.

Event YYYYMMDD	1		2		3		4		
	20040614	Value	Sigma	20050824	Value	Sigma	20070109	Value	Sigma
Start time	2004.453	0.007		2005.648	0.008		2007.024	0.005	
Longitude	E	236.78		236.48			236.28		236.18
Latitude	N	48.06		48.40			48.06		48.20
Slip rate	mm/yr	250.1	164.5	250.6	188.5	251.1	137.5	251.2	138.4
Slip rate	mm/yr	250.5	164.4	250.9	188.5	353.2	137.3	252.3	137.3
Slip rate	mm/yr						299.4		151.5
Poly, 0°	Km	227.6	23.2	219.8	42.2	205.5	25.5	55.3	32.3
Poly, 36°	Km	148.7	12.6	140.3	13.4	131.3	12.1	55.4	23.0
Poly, 72°	Km	68.8	5.8	60.9	11.6	55.0	10.8	55.3	27.1
Poly, 108°	Km	55.2	3.6	55.1	16.5	55.0	5.2	55.4	24.5
Poly, 144°	Km	119.1	4.0	55.8	8.1	97.7	5.4	63.3	10.7
Poly, 180°	Km	189.2	4.9	100.8	6.2	145.5	5.5	115.2	8.0
Poly, 216°	Km	110.1	4.6	180.7	5.8	100.0	4.4	86.9	8.0
Poly, 252°	Km	170.3	18.8	132.7	12.7	135.6	25.4	109.0	17.6
Poly, 288°	Km	90.4	10.0	55.1	12.6	55.8	12.1	55.3	10.9
Poly, 324°	Km	55.1	6.8	61.4	9.8	55.4	6.2	55.2	25.2
Migration rate	km/day	2.0	0.1	5.2	0.5	99.0	94.3	99.0	162.9
Migration az.	degrees	332.5	1.6	330.0	4.7	326.7	56.9	330.0	100.7
Duration	days	18.1		18.1		18.0		25.8	
Amplitude	mm	9.2		9.6		12.8		12.5	
Mw		6.7		6.6		6.7		6.6	
Mo	10^{19} N-m	1.50		1.00		1.34		1.21	
Area	10^4 km ²	5.40		3.60		3.71		3.31	

Poly = radial arm of polygon; with azimuth relative to strike direction. Slip rates are the amplitudes of the triangular time elements. Amplitude is the slip rate integrated over the duration.

Comparison to Szeliga et al. solutions. Figure A5 compares the slip distributions for the 2004 and 2005 events estimated by Szeliga et al . (2008) to the ones estimated here. The moment magnitudes are the same for the 2004 event and differ by 0.1 unit for the 2005 event (lower in this study). The agreement of moments shows that the total integrated slip in the models is the same. Szeliga et al. picked offsets using curve-fitting techniques and then inverted the offsets. Since their Table 1 includes only a few picks and only horizontal component, the extent of slip is difficult to compare (i.e., sites with little slip constrain the extent). Moreover their Table 1 has some errors and omissions, at least for the July 2004 and September 2005 events that are studied here (W. Szeliga, personal communication, 2008).

Solutions with other slip distributions. I did inversions using the 2D Gaussian and 1D Gaussian slip distributions as well as the polygon distribution with other central points. These are not meant to be exhaustive tests but to show the variability that arises from the parameterizations.

The table below shows for each run the slip deficit moment and the amount of moment from slow slip over the 5.6 year period. The **Total** columns are for the entire section of the Cascadia thrust studied (north of 45N). Separate calculations are given for the Olympic Peninsula section (lines 11 to 21 in Fig A2).

In addition, for each run the percent of moment released at depths shallower than 40 km beneath the Olympic Peninsula is given. This depth marks the base of the inter-SSE locked patch (Fig. 2c) and thus the fraction of slow-slip moment shallower than 40 km indicates how much of the slip deficit is released in slow slip. For the inversion described in the paper (P078) 62% of the slow slip was above the base of the locked zone. The other trials show similar or more shallow slow slip.

Table of test runs in terms of moment accumulation and release in slow slip.

run	χ^2_r	#PAR	Total			Olympic Peninsula			OP Shallow (< 40km)		Model description
			deficit	slowslip	%	deficit	slowslip	%	slowslip	%	
			10^{19} N-m	10^{19} N-m		10^{19} N-m	10^{19} N-m		10^{19} N-m		
P073	1.103	304	54.23	5.49	10	24.57	5.02	20	3.30	66	P078, tau = 4 days
P074	1.122	275	52.06	3.78	7	22.90	3.67	16	2.02	55	2D Gaussian
P075	1.106	295	58.42	5.24	9	27.89	5.23	19	4.68	89	Polygon at SC03
P077	1.112	295	57.83	5.95	10	27.55	5.58	20	3.30	59	Polygon at ALBH
P078	1.106	295	54.83	5.05	9	24.20	4.58	19	2.83	62	Polygon
P079	1.120	443	59.19	4.93	8	28.78	4.60	16	4.10	89	1D Gaussian
P137	1.146	234	49.53			20.56					No slowslip

Comparison to 1D Gaussian (p079; Fig. A6). In this inversion the slip distribution was parameterized by a one-dimensional Gaussian function of depth (equation 5). The 19 down-dip profile lines were the same as for the inter-seismic locking model. The number of free parameters here was 443 and $\chi^2_r = 1.120$, an inferior fit compared to the uniform slip model (p078 where $\chi^2_r = 1.106$). Damping of the along-strike variations was applied. The slip distribution shows the patchy nature that characterizes most inversions. This inversion resulted in a large fraction, 89%, of the slow slip above the base of the locked zone

Comparison to 2D Gaussian (p074; Fig. A7). In this inversion the slip distribution was assumed to be a two-dimensional Gaussian distribution (equation 4). The number of free parameters here was 275 and the $\chi^2_r = 1.122$, again a poorer fit than the uniform slip model (p078).

Smaller rise times. An inversion (P073) was run in which the rise times of the time function elements (τ) were set to 4 days instead of 7, and the number of elements for each event were doubled. This resulted in an additional 9 free parameters (compared to run p078) and a slightly smaller $\chi^2_r = 1.103$. Event durations were very close to the earlier values but the moment of the 2005 event increased by about 20% (Event 2) while the moment changes of the others were less than 10%.

Table of duration and moment for run with $\tau = 4$ days.

	Event 1	Event 2	Event 3	Event 4
Duration	days	17.8	17.5	18.1
Mo	10^{19} N-m	1.61	1.23	1.31
				1.34

Alternative polygon centers. For the inversion presented in the paper, the polygon centers were selected based on the highest surface slip. For two runs, the uniform-slip polygon centers were placed beneath site ALBH (P077) and SC03 (P075). The run P075 showed more shallow slip than P077 or P078 (the model shown in the text)

Citations

Fukuda, J., S. Miyazaki, T. Higuchi, and T. Kato (2008). Geodetic inversion for space-time distribution of fault slip with time-varying smoothing regularization, *Geophys J. Int.*, 173, 25-48, doi:10.1111/j.1365-246X.2007.03722.x.

McCaffrey, R., (1995) DEFNODE user's guide, Rensselaer Polytechnic Institute, Troy.
<http://www.rpi.edu/~mccafdr/defnode/>

McCaffrey, R., A. I. Qamar, R. W. King, R. Wells, G. Khazaradze, C. A. Williams, C. W. Stevens, J. J. Vollick, and P. C. Zwick, (2007) Fault locking, block rotation and crustal deformation in the Pacific Northwest, *Geophys J. Int.*, doi:10.1111/j.1365-246X.2007.03371.x.

McCrory, P. A., J. L. Blair, D. H. Oppenheimer and S. R. Walter (2003), Depth to the Juan de Fuca slab beneath the Cascadia subduction margin: A 3-D model for sorting earthquakes: U.S. Geological Survey Digital Data Series, 1 CD-ROM.

Nabelek, J. (1984), Determination of earthquake source parameters from inversion of body waves, Ph.D. thesis, 262 pp., Mass. Inst. of Technol., Cambridge.

Okada, Y., (1992). Internal deformation due to shear and tensile faults in a half-space, *Bull. Seismol. Soc. Amer.*, 82, 1018-1040.

Press, W. H., B. P. Flannery, S. A. Teukolsky, and W. T. Vetterling (1989), Numerical Recipes, Cambridge Univ. Press, Cambridge.

Segall, P. and M. Matthews, (1997). Time dependent inversion of geodetic data, *J. Geophys. Res.*, 102, 22,391-22,410.

Szeliga, W., T. Melbourne, M. Santillan and M. Miller (2008), GPS constraints on 34 slow slip events within the Cascadia subduction zone, 1997-2005, *J. Geophys. Res.* 113, B04404, doi:10.1029/2007JB004948.

Wang, K., Wells, R., Mazzotti, S., Hyndman, R. D., and Sagiya, T., (2003). A revised dislocation model of interseismic deformation of the Cascadia subduction zone, *J. Geophys. Res.*, 108, 2026, doi:10.1029/2001JB001227.

Table of inter-event site velocities.

Site	Longitude °E	Latitude °N	V East mm/yr	σ East mm/yr	V North mm/yr	σ North mm/yr	V Up mm/yr	σ Up mm/yr	Block	Start Year	End Year
ALBH	236.513	48.390	8.1	0.5	7.6	0.5	1.4	0.5	AlbH	2003.20	2008.74
ARLI	237.859	48.174	4.8	0.6	5.0	0.6	0.1	0.6	WhdI	2004.91	2008.57
BLYN	237.073	48.016	7.2	0.5	6.4	0.5	1.2	0.5	Olym	2003.26	2008.74
BREW	240.317	48.132	0.8	0.5	0.2	0.5	-0.1	0.5	EWas	2003.20	2008.74
BTON	237.203	45.486	3.3	0.5	7.5	0.5	0.4	0.5	NoCR	2003.36	2008.53

CHWK	237.992	49.157	4.1	0.5	4.4	0.5	0.0	0.5	SoVI	2003.20	2008.74
CHZZ	236.022	45.487	8.0	0.5	10.9	0.5	2.3	0.5	NoCR	2003.20	2008.74
COUP	237.315	48.217	6.1	0.7	5.8	0.7	0.4	0.7	WhdI	2005.56	2008.57
CPUD	239.686	47.430	1.8	0.7	3.7	0.7	0.0	0.7	Wena	2005.43	2008.57
CPXF	237.744	46.840	4.2	0.5	6.0	0.5	0.3	0.5	Taco	2003.20	2008.74
CVO1	237.504	45.611	3.0	0.5	7.4	0.5	0.2	0.5	Port	2003.20	2008.57
CWAK	238.046	49.153	4.0	0.8	4.4	0.8	0.0	0.8	SoVI	2006.03	2008.57
ELSR	237.240	47.497	6.6	0.6	5.9	0.6	1.0	0.6	Taco	2004.55	2008.57
ENUM	238.046	47.206	3.9	0.6	5.2	0.6	0.1	0.6	YFTB	2004.55	2008.57
FTS1	236.044	46.205	10.2	0.5	11.0	0.5	1.8	0.5	NoCR	2003.20	2008.23
GOBS	239.185	45.839	1.2	0.5	4.2	0.5	0.0	0.5	YFTB	2003.20	2008.74
GWEN	238.672	45.783	1.3	0.5	4.5	0.5	0.0	0.5	YFTB	2003.20	2007.83
KELS	237.104	46.118	4.5	0.5	7.7	0.5	0.5	0.5	Port	2003.20	2007.69
KTBW	237.205	47.547	6.9	0.5	6.0	0.5	1.1	0.5	Taco	2003.20	2008.74
LINH	239.462	47.000	1.8	0.5	3.6	0.5	0.0	0.5	Wena	2003.20	2008.70
LKCP	238.169	47.944	4.4	0.5	4.8	0.5	0.1	0.5	WhdI	2003.20	2008.74
LNGB	237.242	47.219	5.9	0.6	6.2	0.6	0.9	0.6	Taco	2004.47	2008.57
LSIG	238.314	47.696	4.2	0.6	4.7	0.6	0.1	0.6	Seat	2004.58	2008.57
NANO	235.914	49.295	5.5	0.5	6.2	0.5	0.3	0.5	SoVI	2003.20	2008.74
NEAH	235.375	48.298	12.7	0.5	11.2	0.5	2.5	0.5	Olym	2003.20	2008.74
NTKA	233.383	49.592	8.3	0.5	8.6	0.5	2.1	0.5	SoVI	2003.20	2008.56
OTIS	237.663	48.418	5.3	0.5	5.2	0.5	0.1	0.5	SoVI	2003.20	2008.02
P020	241.435	47.001	0.5	0.5	0.0	0.5	0.0	0.5	EWas	2004.46	2008.74
P415	236.270	46.656	8.9	0.6	9.9	0.6	1.7	0.6	Taco	2004.76	2008.74
P420	237.134	46.589	5.7	0.5	7.7	0.5	0.8	0.5	Port	2004.48	2008.62
P421	237.571	46.532	4.3	0.6	7.6	0.6	0.3	0.6	Port	2004.97	2008.74
P432	238.317	46.623	2.7	0.5	4.8	0.5	0.1	0.5	YFTB	2004.47	2008.74
P451	240.959	46.793	0.6	0.6	0.0	0.6	0.0	0.6	EWas	2004.98	2008.74
PABH	235.795	47.213	15.2	0.5	13.7	0.5	0.2	0.5	Taco	2003.20	2008.74
PCOL	237.430	47.172	5.4	0.5	6.0	0.5	0.6	0.5	Taco	2003.56	2008.74
PFLD	237.718	47.899	5.5	0.6	5.1	0.6	0.3	0.6	Seat	2005.25	2008.57
PRDY	237.391	47.391	5.9	0.5	5.7	0.5	0.7	0.5	Taco	2003.66	2008.56
RPT1	237.625	47.388	5.4	0.5	5.4	0.5	0.4	0.5	Taco	2003.20	2008.29
SC00	239.275	46.951	1.9	0.5	3.6	0.5	0.0	0.5	Wena	2003.20	2008.59
SC02	236.992	48.546	6.3	0.5	6.2	0.5	0.4	0.5	SoVI	2003.20	2008.74
SC03	236.296	47.818	11.7	0.5	9.2	0.5	2.9	0.5	Olym	2003.20	2008.74
SC04	236.296	48.924	6.4	0.5	6.6	0.5	0.5	0.5	SoVI	2003.45	2008.74
SEAT	237.691	47.654	5.7	0.5	5.0	0.5	0.3	0.5	Seat	2003.20	2008.74
SEDR	237.776	48.522	5.0	0.5	5.0	0.5	0.1	0.5	SoVI	2003.21	2008.74
SMAI	237.655	47.524	5.2	0.5	5.8	0.5	0.4	0.5	YFTB	2003.73	2008.55
SSHO	237.685	47.682	5.7	0.5	5.0	0.5	0.3	0.5	Seat	2003.20	2008.56
THUN	237.710	47.103	4.8	0.5	5.7	0.5	0.3	0.5	Taco	2003.56	2008.56
TWHL	237.077	47.016	6.1	0.5	6.9	0.5	1.2	0.5	Taco	2003.20	2008.74
UCLU	234.458	48.926	10.6	0.5	9.2	0.5	1.7	0.5	SoVI	2003.20	2008.74
WACO	237.010	45.523	3.8	0.5	7.7	0.5	0.5	0.5	NoCR	2003.20	2008.56
WHD1	237.304	48.313	5.9	0.5	5.7	0.5	0.4	0.5	WhdI	2003.20	2008.28
YAWA	239.495	46.605	1.9	0.5	4.2	0.5	0.0	0.5	YFTB	2003.20	2008.56
ZSE1	237.812	47.287	4.5	0.5	5.5	0.5	0.2	0.5	YFTB	2003.63	2008.74

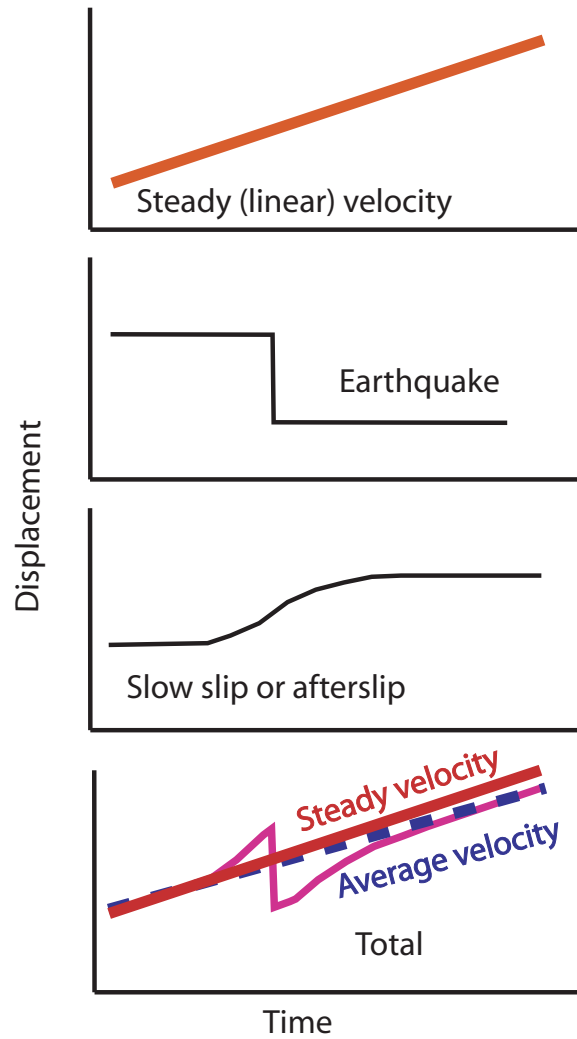
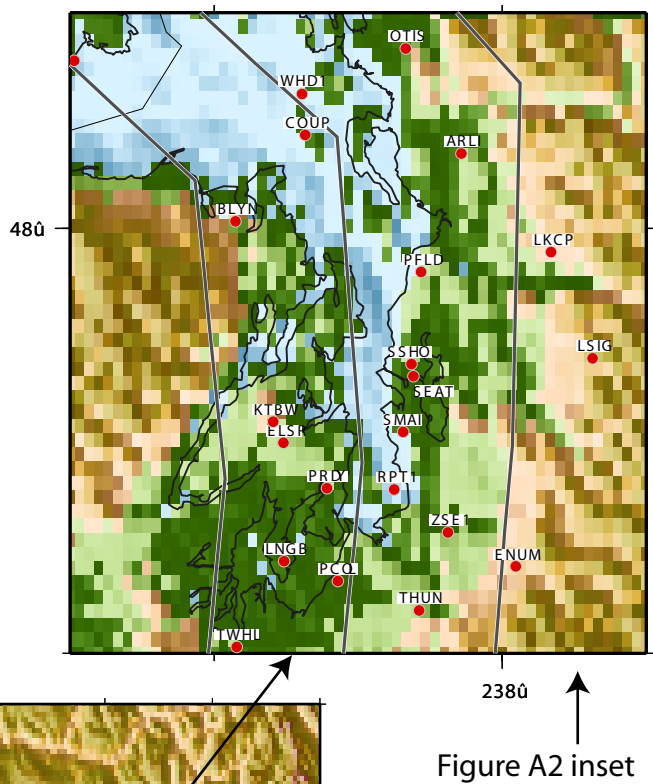


Figure A1 A geodetic time series (purple curve) can be a combination of steady, linear motions and transients such as earthquakes or slow slip events. The average velocity (blue dashed line) can differ from the steady velocity (red solid line) if the transients are not accounted for. The goal of the work here is to separate these signals while imaging their sources.

Figure A2. Map showing GPS sites (red dots with labels), slab countours (labeled at bottom in kms) and nodes (dots). Numbers at deformation front refer to down-dip profiles along slab. Brown lines enclose the region in which moment accumulation and release is compared for inversions. Inset shows close-up of Puget Sound region.



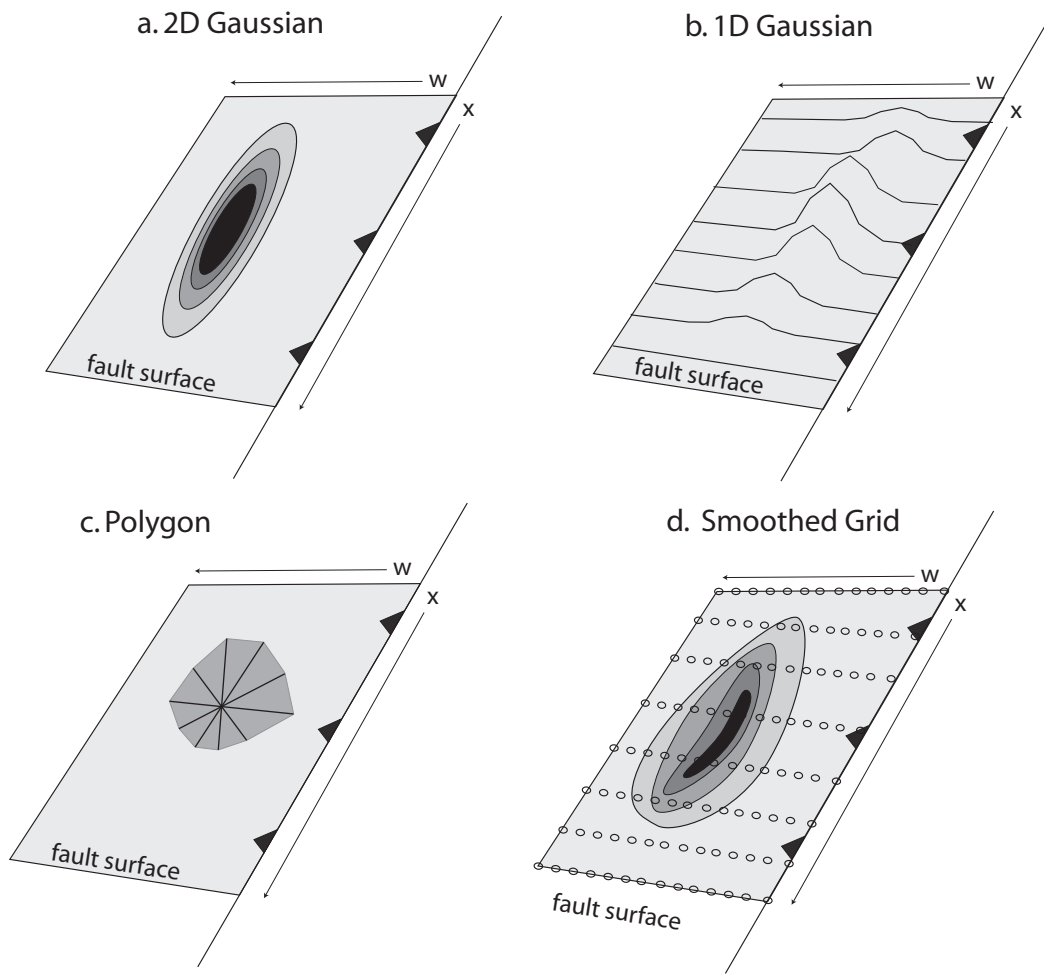


Figure A3. Examples of possible slip distributions used in the inversion. (a) shows a 2-dimensional Gaussian distribution, (b) is a series of 1-dimensional Gaussian distributions in depth, (c) is a polygon of uniform slip, and (d) represents variable slip at a grid of nodes with smoothing applied.

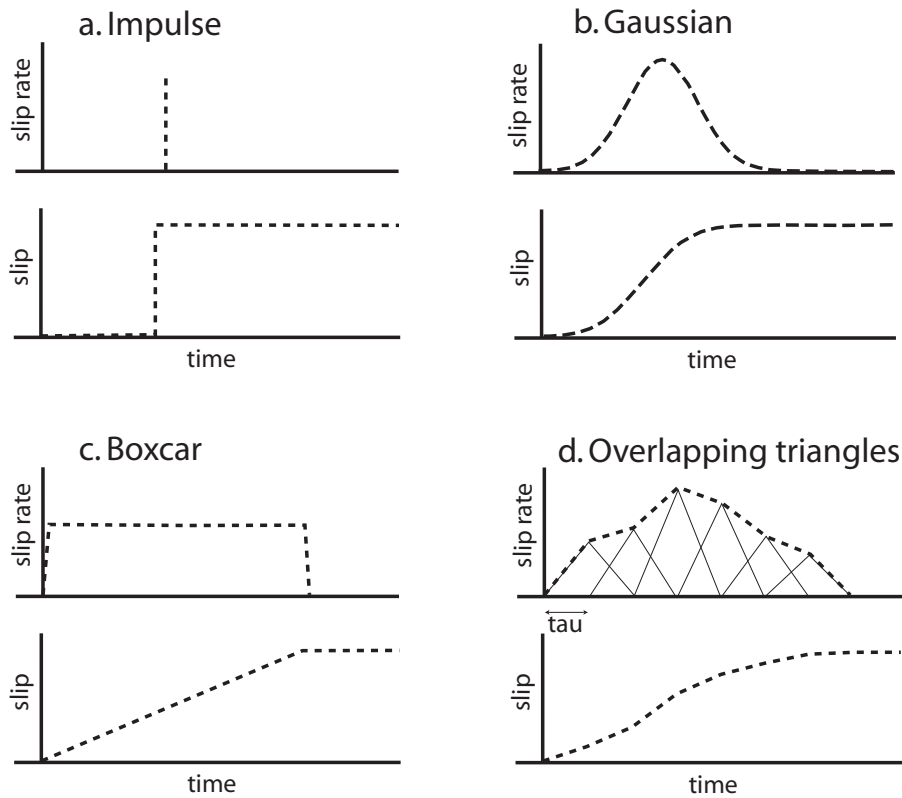


Figure A4. Examples of possible temporal slip distributions used in the inversion. In each case the top panel is the slip rate history on the fault and the bottom is the slip amount determined by integrating the slip rate over time. (a) shows an impulse, (b) is a 1-dimensional Gaussian distribution in time, (c) is a boxcar, and (d) represents variable slip rates by using overlapping triangles. For (d) the triangles are of duration 2τ and overlap in time by an amount τ .

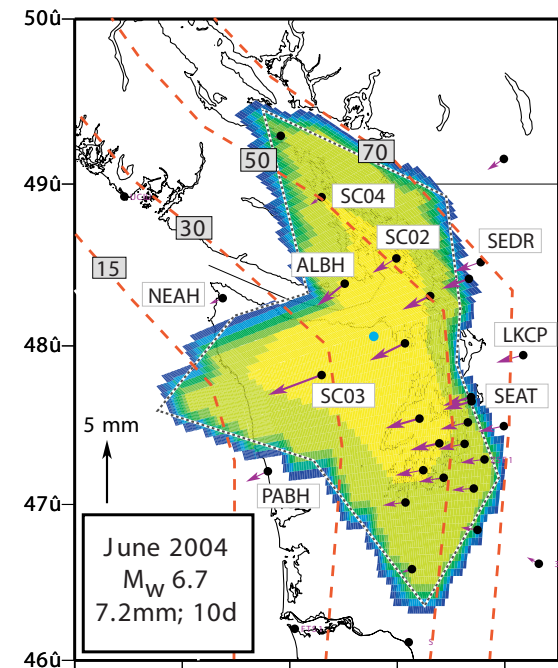
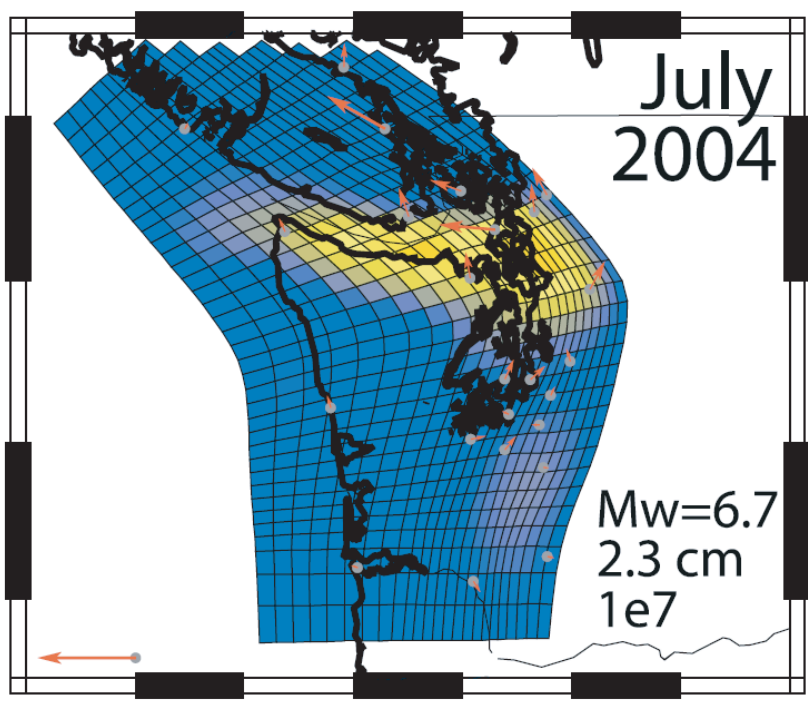
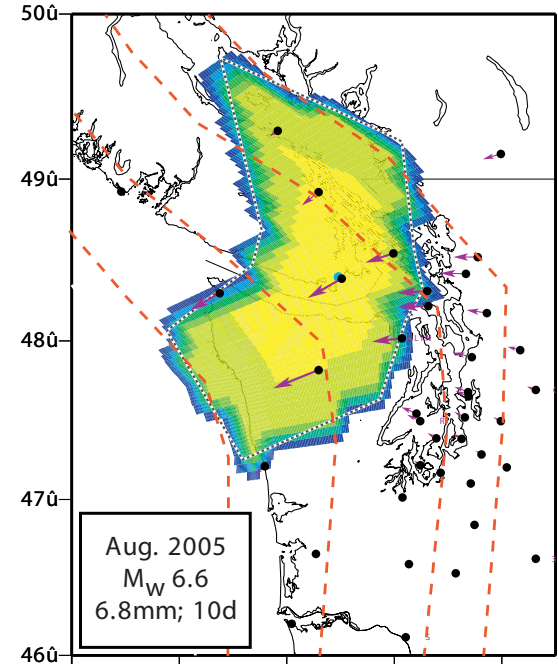
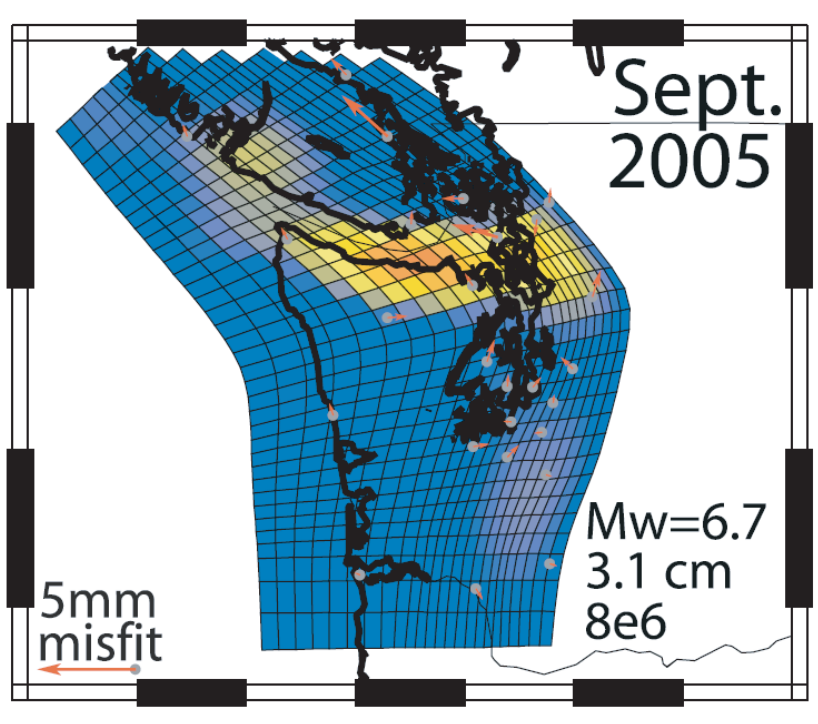


Figure A5. Slip distributions estimated by Szeliga et al. (2008) on left and in this paper on right. Vectors in Szeliga solutions show misfits from picked offsets. Vectors in right panels are surface displacements. Color shading in both represent slip on plate boundary during event.

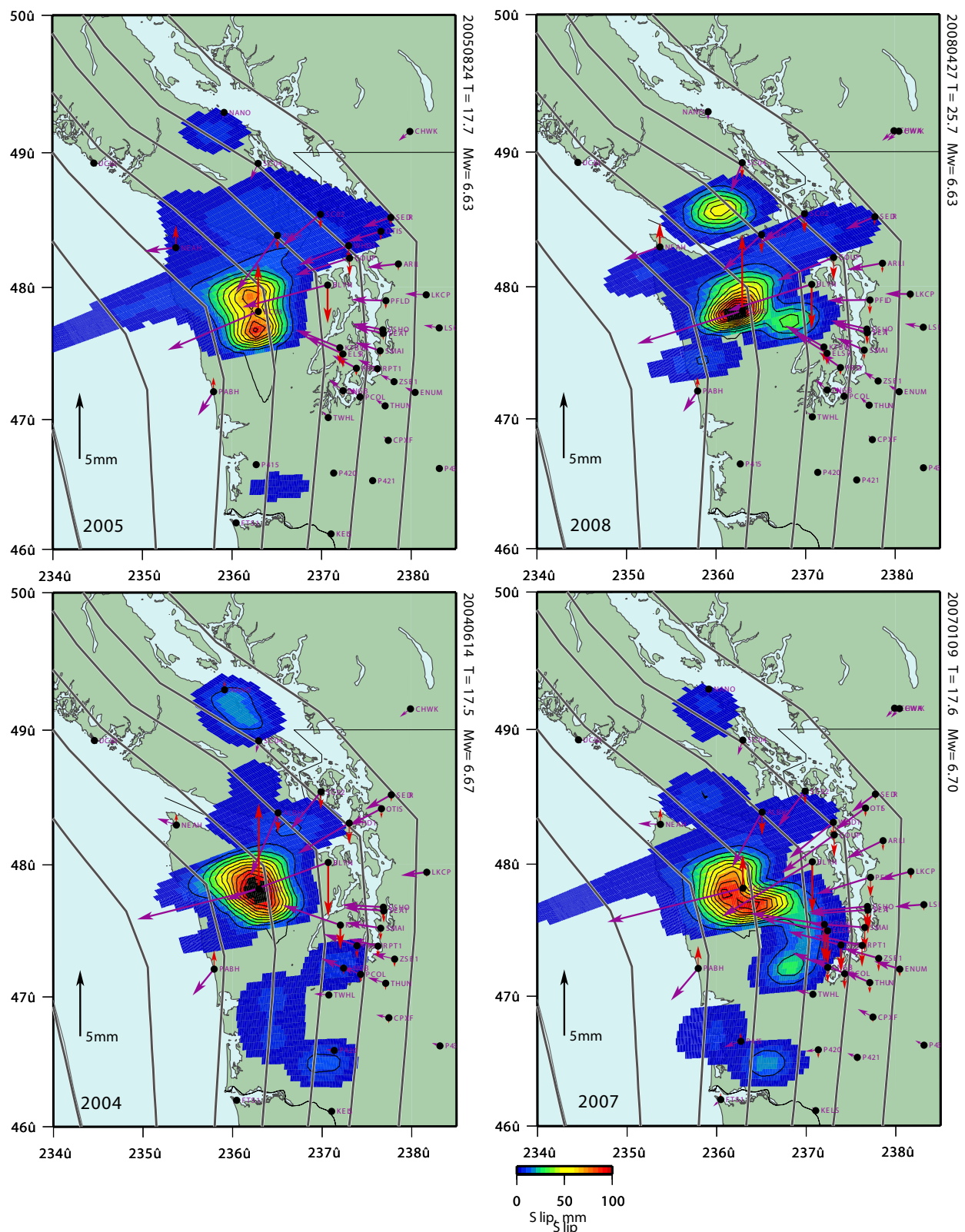


Figure A6. Slip distribution estimated using 1D Gaussian functions of depth. Arrows show expected displacements at surface. Labels to right give start date, duration (T) in days, and Mw.

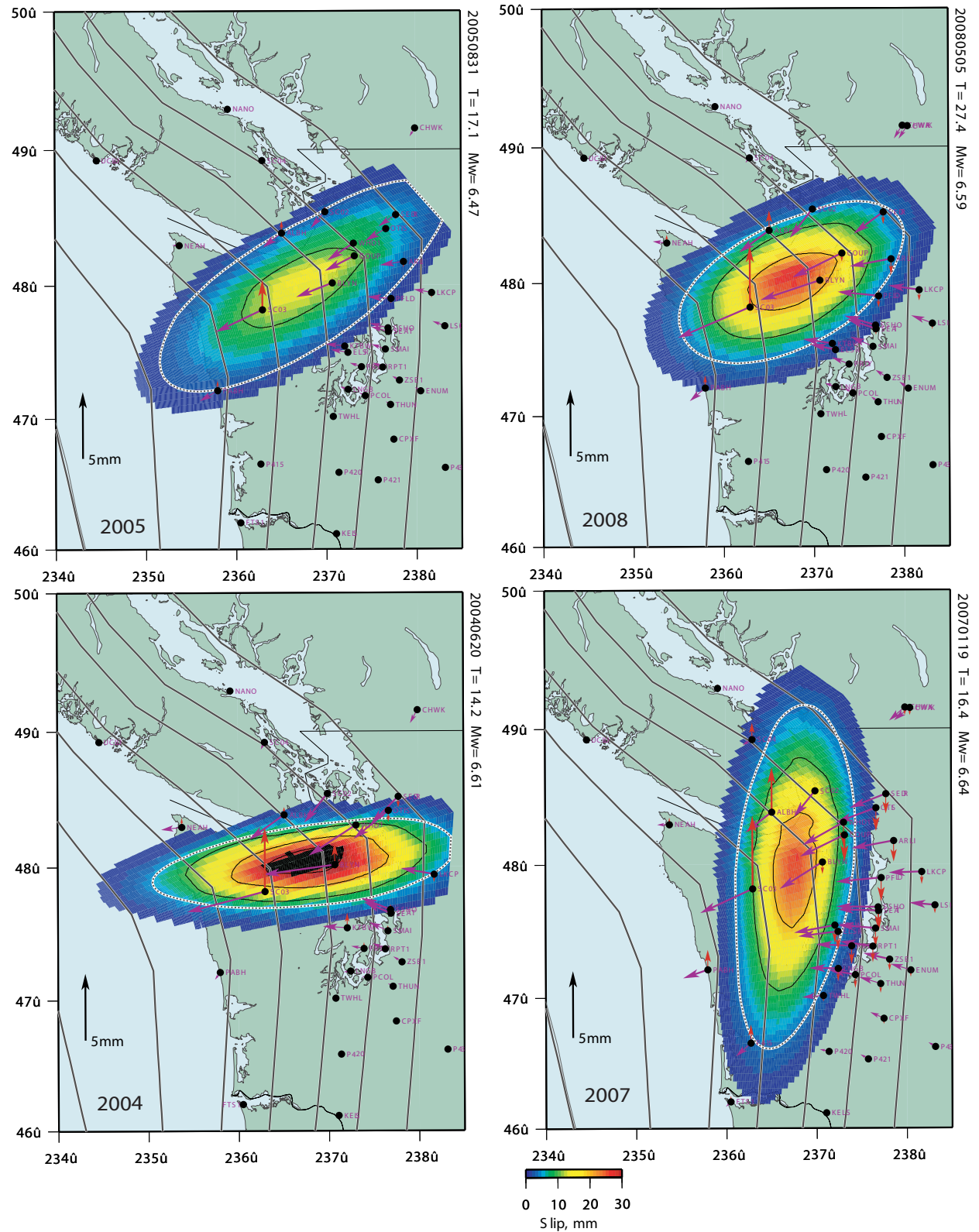


Figure A7. Slip distribution estimated using 2D Gaussian functions. Arrows show expected displacements at surface (red = vertical; purple = horizontal). Labels to right give start date, duration (T) in days, and M_w .